Hydro-mechanical modeling of sinkhole occurrence processes in covered karst terrains during a flood

Li-Hua Luu, Gildas Noury, Zeyd Benseghier, Pierre Philippe

Author-produced version of the article published in Engineering Geology, 2019, 260, 105249.
The original publication is available at https://www.sciencedirect.com/science/article/pii/S0013795219302169
DOI: 10.1016/j.enggeo.2019.105249

Journal

Engineering Geology

Title

Hydro-mechanical modeling of sinkhole occurence processes in covered karst terrains during a flood

Authors

Li-Hua Luu, Gildas Noury, Zeyd Benseghier and Pierre Philippe.

Highlights

- Study case on flood-induced sinkholes during the 2016 meteorological event of Orléans area (France)
- Numerical hydro-mechanical modeling of cohesive soil sinkholes based on field scenarios
- DEM-LBM method for micromechanical approach of internal erosion phenomenon
- Parametric analysis for dropout and subsidence sinkholes processes
- Experimental modeling of sinkhole formation using artificial cohesive materials

Author-produced version of the article published in Engineering Geology, 2019, 260, 105249.
The original publication is available at https://www.sciencedirect.com/science/article/pii/S0013795219302169
DOI: 10.1016/j.enggeo.2019.105249

Hydro-mechanical modeling of sinkhole occurence processes in covered karst terrains during a flood

Li-Hua Luu[a,b], Gildas Noury[a,*], Zeyd Benseghier[b], Pierre Philippe[b]

[a] *BRGM (French Geological Survey), DRP (Risks and Prevention Division), 3 avenue Claude Guillemin, BP 36009, Orléans, 45060, France*
[b] *IRSTEA (National Research Institute of Science and Technology for Environment and Agriculture), RECOVER (Risks, Ecosystems, Vulnerabitily, Environment and Resilience), 3275 route de Cézanne, 13182 Aix-en-Provence, France*

Abstract

Groundwater is an aggravating factor in karstic sinkhole activity as it exacerbates infiltration, percolation, soil saturation and drainage. The exceptionally high number of ground collapses triggered during the major flood of spring 2016 in the Orléans region (France) clearly supports this assertion. In this article, we examine the role of flooding in sinkhole occurrence in cohesive soil layers covering karstified limestone rock. An innovative hydro-mechanical model is applied to simulated field scenarios. Our numerical simulations combine the Discrete Element Method (DEM) to model the solid phase with the Lattice Boltzmann Method (LBM) for the fluid phase. This coupled numerical method allows us to explore the micromechanical features of internal soil erosion in a flood situation. Three processes, consistent with field observations, are simulated and studied through phase diagrams: the formation of a stable cavity within the cover material, the upward propagation of a cavity leading to a dropout sinkhole, and the downward discharge of the granular media, called the subsidence sinkhole. In particular, we perform a parametric analysis of the dropout sinkhole that gives an estimate of the collapse width. In the first approximation, the characteristic length is shown to increase linearly with cover thickness, regardless of the other main parameters (soil cohesion, hydraulic head, system geometry).

*Corresponding author
Email address: G.Noury@brgm.fr (Gildas Noury)

Finally, we present an exploratory experimental study, using sand with artificial cohesion that successfully reproduces different erosion regimes predicted by our numerical simulations.
Keywords: cover-collapse sinkhole; flood; karst terrain; cohesive soil erosion; hydro-mechanical modeling.

---

1. Introduction

Karstic landscapes cover around 15-20 % of the Earth's surface and are a matter of concern for land-use, especially for sinkhole hazards (Ford and Williams, 2013). Cover by limestone karst is one of the most critical environments (Sowers, 1996; Waltham et al., 2008), mostly located in easy-to-build flat areas (such as alluvial plain). The subterranean configuration is often inaccessible (filled or underwater entries) while the non-karstic lithology of the cover seems "stable". Large urbanized areas have been built on this kind of karst cover soil, the most prominent examples being Florida in the USA, the Gauteng Province in South Africa, and the Orléans area in France. Hazard and risk assessment for the safety of people and property appears difficult and remains limited to the locations of recent sinkholes and the use of archives to localize old refilled sinkholes. The Florida Office of Insurance Regulation estimated an average economic loss of 280 million per year due to sinkholes during the period 2006 to 2010 (Kuniansky et al., 2016).

The main process leading to sinkholes in karst cover is soil piping, defined as down-washing of the material cover into the network of limestone cavities *via* water circulation (Beck, 2012). Moreover, karst cover soil is particularly hazardous in the case of intense rainfall and floods (Brinkmann et al., 2008; Gutierrez et al., 2014; Hyatt and Jacobs, 1996). In France, the meteorological event that occurred in spring 2016 is a new example of the impact of intense rainfalls and floods on sinkhole occurrence (Noury et al., 2018). The lessons learned from this event enabled the French Geological Survey (BRGM) and the National Environment and Agriculture Research Institute (IRSTEA) to improve

insight into internal erosion processes through innovative numerical modeling.

This article originated from this case study, thus it focuses on sinkhole formation during floods. This process is still poorly understood: some experiments have succeeded in reproducing simple configurations (Perez et al., 2017) but numerical models are rare or do not take into account the complexity of the influence of water circulation. Few studies address the complexity of cavity development within the cover deposit. The main approach adopts continuum mechanics schemes (often using FLAC software) to simulate the geomaterial system using constitutive models, typically incorporating visco-elasto-plastic rheology (Baryakh and Fedoseev, 2011; Shalev and Lyakhovsky, 2012). With the same type of numerical method, recent studies have benefitted from adding hydro-mechanical coupling to take into account water leakage and drawdown (Rawal et al., 2017; Tao et al. 2015). Although this kind of analysis allows modeling the general failure of an opening void (Mohr-Coulomb envelope), it cannot predict local failures such as block dislocation.

All fluid-soil interactions in cover-sinkholes are related to the widespread phenomenon of soil erosion. In particular, the expansion of underground cavities is very similar to the backward erosion piping observed in the foundations of hydraulic works (Bonelli, 2013). In this field of application, studies are at a more advanced stage, notably in experimental research (Sellmeijer et al., 2011; Wilson et al., 2015). With regard to numerical investigation, the last few years have seen substantial progress in the micromechanics of geomaterials which allow the discrete description of soils, especially with the Discrete Element Method (DEM) developed by Cundall & Strack (1979). DEM, based on the realistic mechanical modeling of a large number of individual particles, has become one of the most increasingly used methods for the numerical simulation of soils in geomechanics (Radjaï, 2011). To this end, coupling schemes have been specifically developed to obtain fluid flows at the pore scale (Cuellar et al., 2015; Lominé et al., 2013; Luu et al., 2017; Ngoma et al., 2018; Tran et al., 2017).

In this paper, we study sinkhole occurrence in covered terrains, using both field observations after floods and micromechanical modeling of the phenomenon

at the scale of fluid-particle interaction. Section 2 reports on the case study of the Orléans region which was subject to massive rainfall in 2016. An unusual number of sinkholes surveyed in one of the flooded areas and hypothetical scenarios are presented. Section 3 is dedicated to our numerical modeling of cohesive soil layer destabilization triggered by hydraulic load. After presenting the coupled numerical method that combines the Lattice Boltzmann Method (LBM) for describing the fluid phase and the Discrete Element Method (DEM) for the solid phase, we present typical simulations that determine the phenomenology of the sinkhole formations. Different analyses from a parametric study are proposed, notably based on phase diagrams for the direct estimation of collapse. Then, we propose an experimental method using model granular media able to qualitatively reproduce the processes observed in simulations. We finally end the paper with a broad conclusion and perspectives.

2. Case study: the 2016 meteorological crisis on sinkholes activity in the Orléans area (France)

2.1. General context

Orléans is a city in the Loire Valley located 130 km south of Paris (Fig. 1). The geological bedrock of the Orléans area is constituted by the Beauce limestone (50 to 90 m thick Tertiary lacustrine limestone) (Lorain, 1973). The limestone of the Loire floodplain is mantled by Quaternary alluvium (5 to 15 m thick) and the groundwater level is close to the ground surface (5 m deep). These areas are known to be underlain by an extensive karstic cave network (Perrin et al., 2017). However, our knowledge of network configuration is poor due to limited speleological investigations (few entrances, water-filled karst) (Moreau, 2002). The current activity in the Beauce limestone karst is attested by sinking streams, spring locations, caves found in bore holes, and the occurrence of sinkholes. Since 1903, assessments have reported approximately 640 sinkholes in the 170-km Loire floodplain around Orléans, usually called "Val d'Orléans" (Perrin et al., 2017). The latest report mentions a rate of 3 to 4 per year.

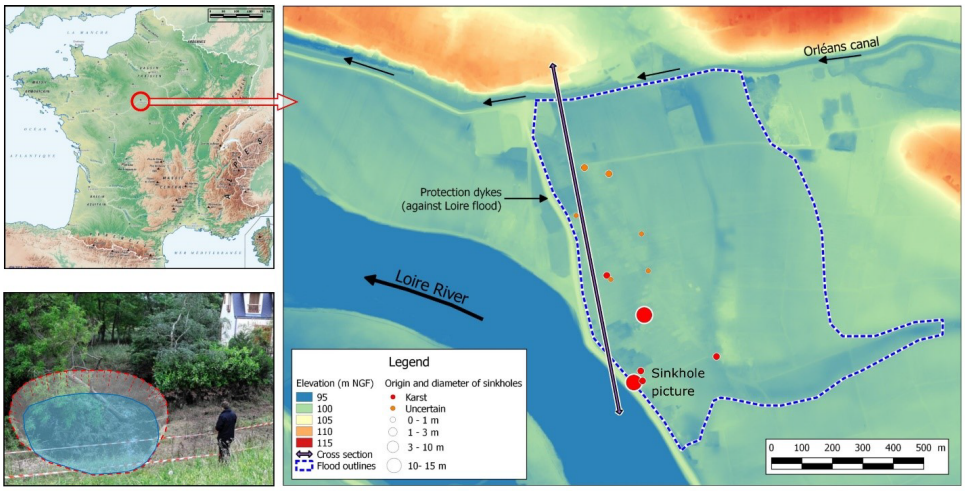

Figure 1: Map of general context of the Orléans (Chécy area) indicating sinkholes triggered by the 2016 flood.

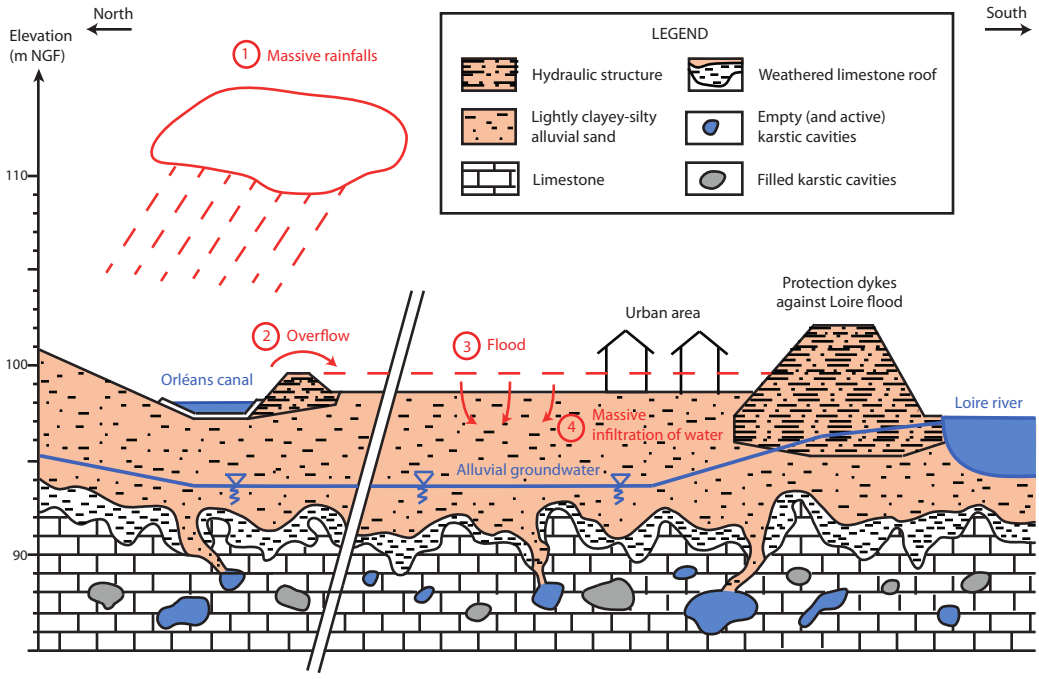

Figure 2: Geological cross section through the Loire floodplain in Chécy area and sketch of the cascading effects caused by the 2016 flood (see text).

Mean sinkhole frequency is therefore approximately 0.02 to 0.03 occurrences per square kilometer per year.

At the beginning of June 2016, the northern part of France, including the Orléans area, endured a major meteorological crisis. Figure 2 provides an illustration of the cascading effects: 1) During the massive rainfalls, about 140 mm of water was recorded over 5 days, the equivalent of three normal rainy months. 2) The overflow of an artificial canal spread the flood over a 1-km^2 area. 3) The Loire floodplain was flooded by 1 to 2 m of water, covering a recently built neighborhood, the water-treatment plant and several fields for 10 days. 4) This exceptional situation led to the massive infiltration of water. The small town of Chécy was particularly hard hit. There, twelve sinkholes formed immediately or a few days after the meteorological event (Fig. 1). Considering the geological terrains affected and whose main components are presented in Fig. 2, most of these sinkholes were associated with karst collapses.

2.2. Detailed analysis of flood-induced sinkholes in the Chécy area.

The frequency of flood-condition sinkhole occurrence (spatial and temporal) is unusually high: 12 sinkholes in 1 km^2 during the 10-day flood correspond to a sinkhole occurrence rate of 450 events per square kilometer per year. The sinkhole occurrence rate evaluated in normal condition (0.02 to 0.03 per square kilometer per year), is thus multiplied by a factor from 15,000 to 22,000 because of flooding.

Figure 3 shows pictures from BRGM field surveys after floods. We can distinguish two different "post-mortem" shapes of sinkholes: the hourglass shape and the inverted bowl/ teardrop shape usually associated with cover material that is non-cohesive and cohesive, respectively (Waltham, 2008). The soil of Val d'Orléans is mainly a slightly cohesive clayey-silty sand and both shapes are usually observed in normal conditions. In the area studied, most of the twelve sinkholes triggered by the 2016 flood had an hourglass shape.

Figure 4 shows the mean diameter of the twelve sinkholes as a function of floodwater level. They all have a similar size, except two singular bigger

Figure 3: "Post-mortem" shapes of flood-induced sinkholes in Chécy area.

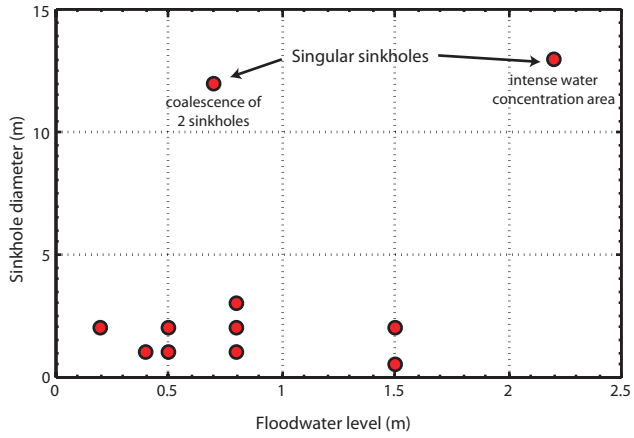

Figure 4: Influence of floodwater level on sinkhole diameter analysis in the Chécy area.

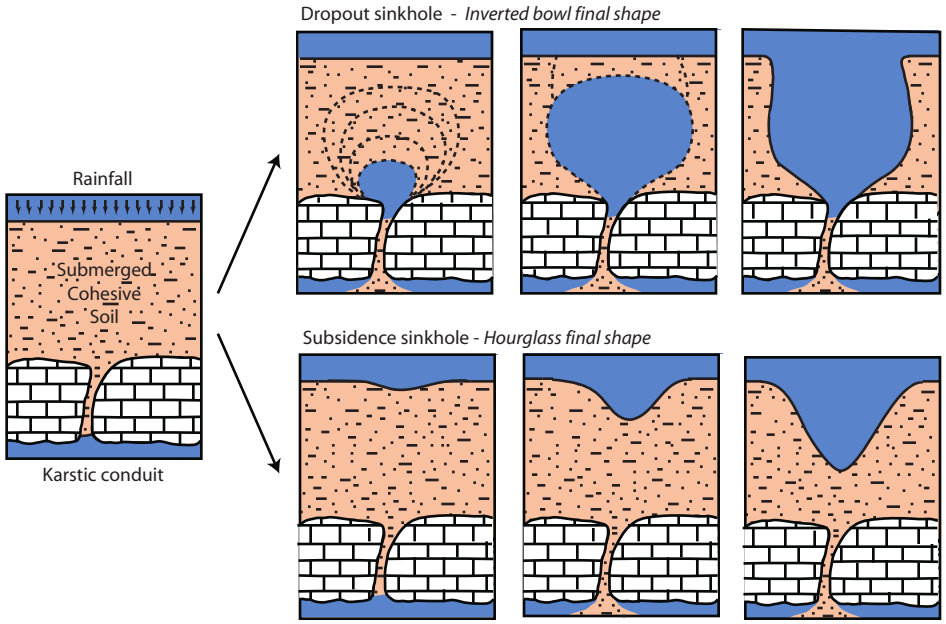

Figure 5: Scenario in the flooded (fully saturated) situation: dropout sinkhole and subsidence sinkhole, leading to inverted bowl and hourglass final shapes, respectively.

sinkholes. One of the latter is located in an intense water-flow concentration area and the other is assumed to have resulted from the coalescence of two neighboring sinkholes, explaining their larger size. So, apart from these two cases, we can therefore consider that the floodwater level does not seem to substantially influence sinkhole diameter, which is between 0.5 m and 3 m. By contrast, the mean diameter of holes in normal conditions is between 1 and 2 m. Mention can also be made of a marginal case: the biggest recent sinkhole was 16 m in diameter and 7.5 m in depth. It occurred in 2010 without flood at Saint-Pryvé-Saint-Mesmin and destroyed a house, fortunately without casualties.

2.3. Field scenarios of sinkhole processes

The flood-induced downward water flow within the soil is assumed to have increased the suffosion phenomenon [1], which consists in the down-washing of alluvium by water towards cavernous bedrock with relatively small and poorly connected voids (not necessarily well-developed and integrated in karstic cave networks). From this elementary mechanism of soil migration, we hypothesize two different erosion processes leading to the two different final sinkhole shapes presented above. Figure 5 represents a cohesive soil layer over karstic conduits in the flood-condition. The first scenario is similar to the dropout sinkhole, commonly reported in the classical non-submerged case, where a cavity expands from the underground up to the collapse of the roof, leading to an inverted bowl sinkhole shape. Geotechnical results commonly used by engineers for the construction of foundations in karstic terrain, show that the potential collapse diameter is $2/3$ the height of the overlying soil layer (Sowers, 1996). In a flood situation, this prediction could change. Notably, the water load could trigger the final collapse of the thin residual layer. The second scenario is similar to that of the subsidence sinkhole, in which soil destabilization starts at the surface and results in an hourglass shape. It is noteworthy that this process is usually attributed to cohesionless soil (DeWaele et al., 2011; Waltham, 2008). However, the following modeling work will demonstrate that this unexpected scenario (for cohesive soil) is quite plausible. Numerical simulations will show that exceptional vertical water flow might be responsible for intense erosion according to this second process.

3. Numerical modeling

This section presents a numerical study of sinkhole formation triggered by floods, according to previous scenarios deduced from the *in-situ* observations

[1] Suffosion is distinguished from *suffusion*, which is an internal erosion mechanism that implies the detachment of fine particles in the pore space of a matrix composed of larger particles.

presented in Figure 5. To tackle this problem from a physical perspective, we propose to bridge the gap between the micromechanical phenomena at the grain scale and the macroscopic process of the cover-collapse sinkhole, by numerically investigating the interactions between a fluid phase and the solid phase for a large assembly of bonded particles. The main objective is to explore the different erosion regimes by varying the soil properties, including cohesion, and hydrodynamic conditions through a parametric study.

3.1. Micromechanical approach

Advanced research in geomechanics demonstrated that a subtle difference in microstructure could lead to significant changes at the macroscopic scale, notably by triggering hydro-mechanical instabilities such as gravitational slope failure (Iverson, 2000) and liquefaction (Benahmed et al., 2004). To study soil erosion involved in sinkhole formation, we used a 2D numerical model that combines the Lattice Boltzmann Method (LBM) for describing the fluid phase and the Discrete Elements Method (DEM) for the solid phase. An increasing number of numerical studies rely on this coupling to treat multi-scale geo-mechanical problems (Cuellar et al., 2015; Lominé et al., 2013; Luu et al., 2017; Ngoma et al., 2018; Tran et al., 2017).

3.1.1. Solid phase modeling: Discrete Element Method (DEM)

The DEM method, initially developed by Cundall and Strack (1979), is used here to implement the mechanical behavior of a 2D assembly of circular particles whose trajectories are described by Newton's equations of motion. The particles interact through contact forces, each of them being decomposed into a normal force F_n and a tangential force F_t (see Fig 6). These two components are given by a viscoelastic Kelvin-Voigt model and a viscous-regularized Coulomb law, respectively. Also, the interaction moment M is defined by the tangential force with the particles' radii as lever arms. To account for interparticle cohesion, we consider a parabolic yield volume in the space of contact forces and moment, as developed by (Delenne et al., 2004). In the present numerical model, traction,

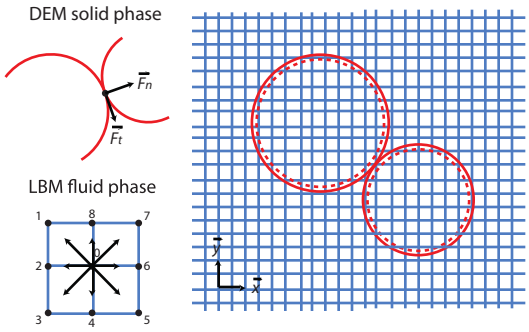

Figure 6: Illustration of the 2D coupled numerical method: DEM frictional contact model and LBM D2Q9 scheme (see text).

shear and bending yield thresholds are assumed to depend only on a unique force C which represents the mean interparticle bond strength. Finally, the model is enriched by an additional damage model adapted from Silvani *et al.* (2009), which prescribes a progressive degradation of cohesive strength for subcritical stresses, namely those contained within the yield volume. For more details, the reader can refer to a previous numerical study performed with this DEM cohesion model (Cuellar et al., 2015).

3.1.2. Fluid phase modeling: Lattice Bolzmann Method (LBM)

The LBM method, based on Boltzman's kinetic theory of gases, describes the statistical behavior of a large population of fictitious fluid particles moving randomly. The fluid flow is simulated by solving the discretized Boltzmann equation for the probability density function $f(\vec{x}, \vec{c}, t)$ to find a particle at a position $\vec{x}$ with the lattice speed $\vec{c}$ at the given time t. The fluid dynamics occurs as the result of propagation and collision of the fluid particles over a discrete regular lattice. To compute this process, the present code uses a Two-Relaxation-Time model (TRT) (Talon et al., 2012) and a classical D2Q9 scheme that involves a finite 2D lattice grid with 9 directions at each grid point (including that staying at the current position, see Fig 6) (Lallemand and Luo, 2000; Yu et al., 2003). For a given kinematic viscosity ν and fluid density ρ_f and an adapted choice of LBM relaxation times, a Chapman-Enskog expansion gives

Table 1: Parameters used in the numerical simulations

Solid phase		Fluid phase	
Mean radius, r	$1.5{\cdot}10^{-3}$ m	Kinematic viscosity, ν	$4{\cdot}10^{-5}$ m^2/s
Polydispersity, $r_{\max}/r_{\min}$	1.5	Lattice speed, c	10 m/s
Bond strength, C	10 N, 20 N	Inlet pressure, P_{inlet}	[1-34] kPa
Solid density, ρ_s	$2.5{\cdot}10^3$ kg/m^3	Fluid density, ρ_f	$1{\cdot}10^3$ kg/m^3
Geometry			
Length, L	$23.7{\cdot}10^{-2}$ m, $40{\cdot}10^{-2}$ m		
Height, H	$[8.5\text{-}18.5]{\cdot}10^{-2}$ m		
Orifice size, Δ	$[15\text{-}75]\ {\cdot}10^{-3}$ m		
Conduit height	$6{\cdot}10^{-2}$ m		

the incompressible Navier-stokes equations, and then the direct derivation of the macroscopic features of the flow in the low Mach number limit, namely for $Ma = \frac{V_{\max}}{c} << 1$, where $V_{\max}$ is the maximum fluid velocity and c the lattice speed.

3.1.3. Fluid-solid interaction

To couple the DEM and LBM methods, we assign a fluid or solid status at each LBM grid point that is updated at each LBM time step (with 2 DEM subcycles per LBM cycle). The space resolution for our simulations is fixed so as to have a mean particle diameter equal to 10 LBM nodes. In the LBM code, when a velocity vector is directed towards a node assigned as solid, we use a typical bounce-back algorithm for which the fluid vector basically reverses its direction to obtain a no-slip condition at any solid surface (grains and walls). To compute the hydrodynamic forces on grains, we refer to a relationship developed by Bouzidi *et al.* (2011) based on a momentum-exchange between fluid and solid nodes. Finally, the LBM calculation is implemented with a hydraulic radius (dashed circles in Fig. 6) equal to 0.8 times the real radius used in DEM. In this way, the fluid can flow between the disks of the DEM assembly and we recover non-zero permeability in our 2D granular configuration.

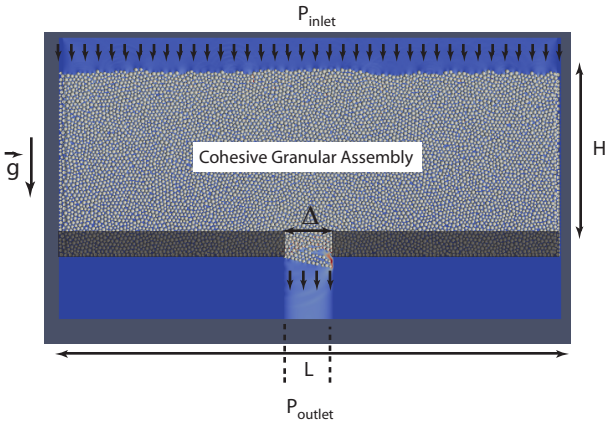

Figure 7: Numerical model for a sample with 7000 particles of mean radius r=1.5 mm (H=13.5 cm, L=40 cm, P_{inlet}=5 kPa and Δ=3 cm) at t=0.6 s from the triggering of the pressure gradient. The particle cohesion number is Coh=95, except in the dark grey zone of 1.5 cm thickness, where the cohesion is 10 times greater in order to represent a more realistic boundary condition than a wall.

3.2. Application to sinkhole formation

3.2.1. Numerical model setup

In a preliminary work, we reproduced the process of collapse in a clogged underground conduit under high hydraulic gradients (Luu et al., 2017) and hence demonstrated the relevance of employing DEM-LBM coupling to investigate the different scales involved in soil erosion, from behavior at the grain scale to the erosion front kinetics, by going through the mesoscale of force chains. In the present study, we focus on cover-collapse sinkhole formation in a homogeneous soil layer (i.e. without weaker zones). As presented in the previous section and illustrated in Figure 5, we intend to reproduce the flood-induced collapse of a cohesive sediment layer overlying karst caves or open fissures in the bedrock, according to representative scenarios for the geological context of the Orléans case study.

Our numerical model consists of a fully immersed cohesive granular layer, at the bottom of which lies an orifice through which water flows freely, assuming underneath a connection to the underground conduit of a hydraulic network

(Fig. 7). To induce erosion processes, we impose a high enough pressure at the sample upper surface P_{inlet}, keeping the outlet pressure at zero. For this study, we implement a cohesive assembly of particles whose mean radius is r=1.5 mm. We vary the height H and the length L of the 2D granular samples, corresponding to assemblies of 4835 to 9636 particles, while the size of the orifice Δ ranges from 10 to 50 times the mean particle radius. All the numerical simulation parameters are given in Table 1 (note that the particle parameters are similar to those of usual 2D-DEM numerical studies).

To quantify soil cohesion, we define a dimensionless particle cohesion number as the ratio of the bond strength C to the particle's own buoyant weight, $Coh = \frac{C}{(\rho_s - \rho_f) g S}$, where $\rho_s - \rho_f$ is the submerged apparent density, g is the gravitational acceleration and S is the particle's surface (2D model). It is noteworthy that here particle cohesion consists of solid bonds with irreversible failure, and is different from the macroscopic cohesion classically defined through the Mohr-Coulomb failure criterion. The range of Coh studied is equivalent to a weakly cemented granular matter. Regarding flow regime, the Reynolds number can be measured within the bottom conduit before the detachment of the grains, such that $Re = \frac{\bar{V}\Delta}{\nu}$, where $\bar{V}$ is the fluid mean velocity and ν the fluid kinematic viscosity. Globally, in the granular assembly and outside, $\bar{V}$ is of the same order of magnitude as the maximum fluid velocity V_{max}, ranging from 0.01 to 1 m/s. For reasons of computation time, the particle size is taken substantially larger than in reality. Therefore, we use a higher viscosity than water to simulate realistic flow regimes by obtaining similar Reynolds numbers to those in the field. Thus, all the following simulations reproduce flow regimes that are laminar and incompressible, with an Re from 30 to 600 and a Mach number $Ma = \frac{V_{\text{max}}}{c}$ smaller than 0.1.

3.2.2. Phenomenology

We performed a parametric study using our DEM-LBM code to investigate erosion processes according to two different micromechanical viewpoints: from the bonds within the cohesive granular sample and from the local stress field.

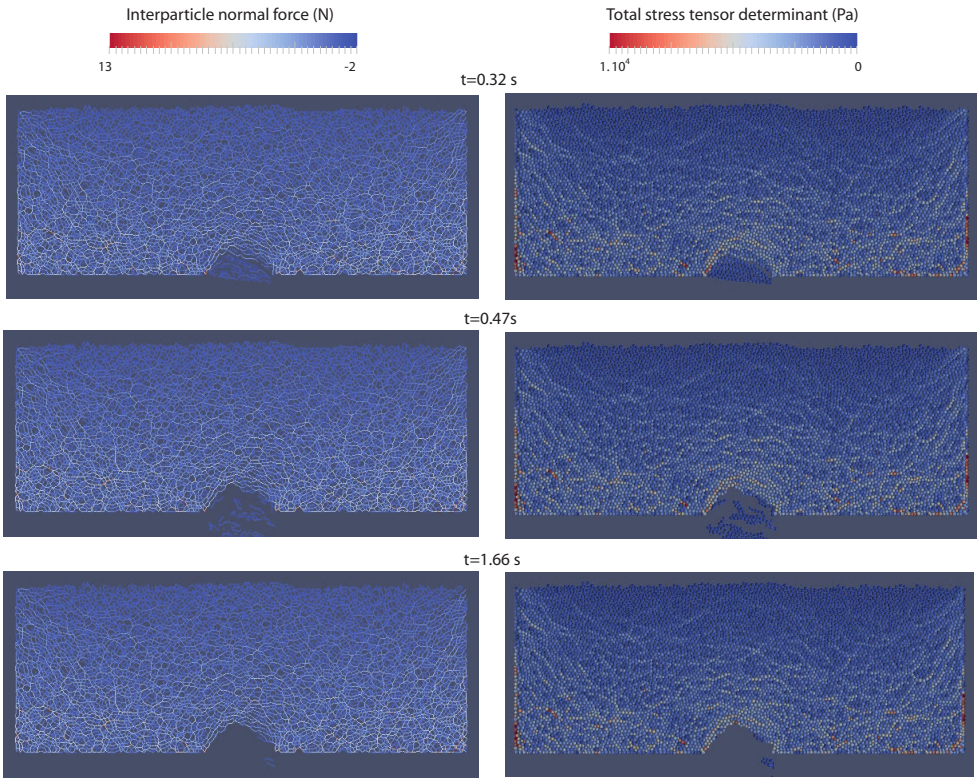

Figure 8: Cavity formation for a sample with 7000 particles of mean radius r=1.5 mm (H=13.5 cm, L=40 cm, P_{inlet}=0.5 kPa, Δ=4.5 cm, and Coh=95) with evolution of the microstructure over time: normal interparticle force (left) and total stress determinant (right).

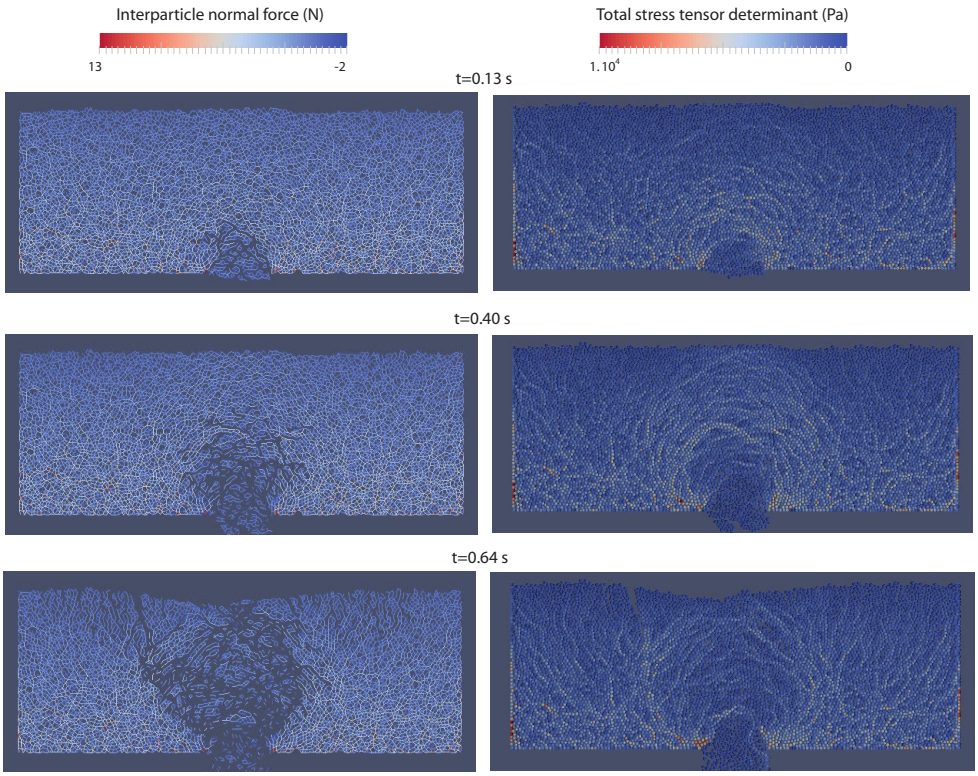

Figure 9: Dropout sinkhole for a sample with 7000 particles of mean radius r=1.5 mm (H=13.5 cm, L=40 cm, P_{inlet}=1.0 kPa, Δ=4.5 cm, and Coh=95) with evolution of the microstructure over time: normal interparticle force (left) and total stress determinant (right).

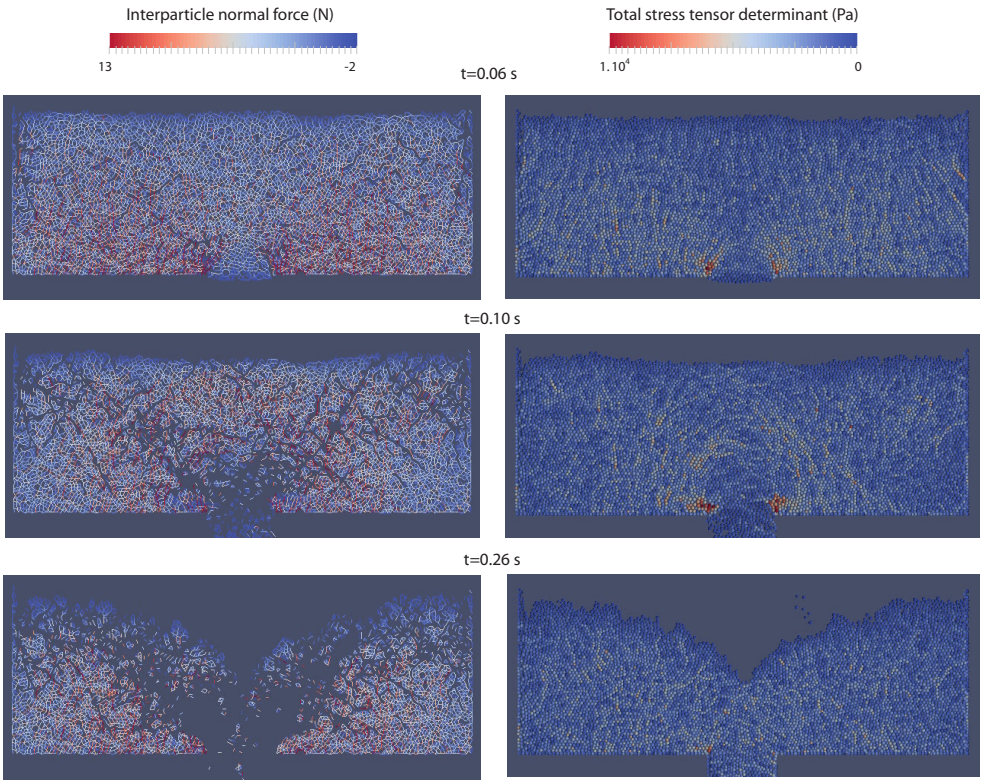

Figure 10: Subsidence sinkhole for a sample with 7000 particles of mean radius r=1.5 mm (H=13.5 cm, L=40 cm, P_{inlet}=9.6 kPa, Δ=4.5 cm, and Coh=377) with evolution of the microstructure over time: normal interparticle force (left) and total stress determinant (right).

The following figures (Fig. 8, 9, 10) present typical simulations of microstructure evolution over time regarding: on the left side, the interparticle normal force network composed of positive (compressive) and negative (tensile) normal forces. On the right side, the total stress tensor for each grain, as the contribution of both the stress exerted by the neighboring particles in contact and the hydraulic stress of the surrounding fluid. We choose the stress tensor determinant to quantify this magnitude.

The first erosion regime is illustrated in Figure 8. From the bottom orifice we observe an evacuation of grains that stops early, leaving a stable cavity. This is a marginal regime also simulated in our previous work on clogged underground conduit collapse [21]. This vault cavity recalls quasi-static intermittent void formations in quasi-static and non-flooded conditions, commonly described in geotechnical works (Sowers, 1996).

Then, when increasing the hydraulic load (P_{inlet}), or enlarging the bottom orifice (Δ), or decreasing the interparticle cohesion (Coh), we observe the expected backward erosion implied in the dropout sinkhole. Figure 9 (left) shows how interparticle bonds progressively break from the orifice to the surface. In the early stages, there is no disturbance of the grains at the top. Subsequently, the destabilization front moves along a direction opposite the flow direction (namely the "backward" direction). We therefore observe a damage zone that gradually develops upward, leading to the first scenario proposed in Fig. 5. The granular medium self-organizes by creating force chains under compression. Subjected to a traction mechanism, the erosion process takes place through the progressive breaking of arches sustained by force chains. Indeed, the total stress computation in Figure 9 (right) gives a qualitative representation of how the force chains (displayed by the highest values) are involved in the erosion kinetics. The upward front advances in a series of vault-to-vault movements. Thus, our numerical model approximately simulates the inverted bowl shape for the destabilization zone, hypothesized in Section 2. Note that the cavity formation could be included in this backward erosion regime. It is actually likely that, given a sufficient amount of simulation time, the cavity could expand up to the

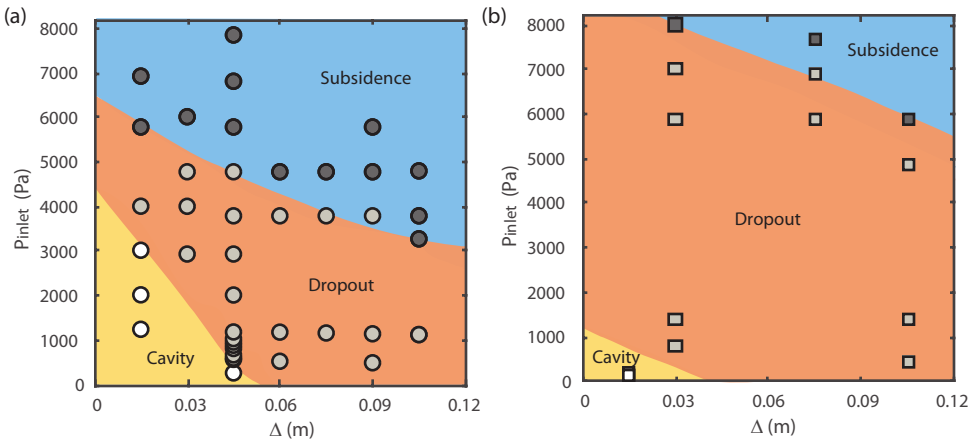

Figure 11: Phase diagrams related to the inlet pressure P_{inlet} and the orifice size Δ, (a) for Coh=95, H=13.5 cm and L=40 cm. (b) Idem for Coh=95, H=8.5 cm and L=40 cm.

surface by intermittent periods of grain evacuation.

Lastly, if the erosion parameters continue to increase (increasing P_{inlet}, increasing Δ and decreasing Coh), a continuous discharge regime is recovered, similar to the subsidence sinkhole previously presented as the second speculative scenario in Figure 5. In Figure 10 (left), we observe that the evolution of the interparticle force network presents fracturing initiated along two dislocation lines, forming a cone, and which propagates rapidly almost throughout the granular sample. The evacuation of grains through the orifice leads to the subsidence of the surface, contrary to the previous backward erosion. This regime is very similar to the hourglass and hopper, two classical granular matter problems. But in our case, we added interstitial fluid flow and interparticle cohesion. This regime of downward migration of cohesive particles (which is not usual in geotechnics, see previous Section in 2.3) has been recently studied numerically using CFD-DEM coupling (Liu et al., 2018), but no experimental work has been dedicated to this phenomenon to our knowledge.

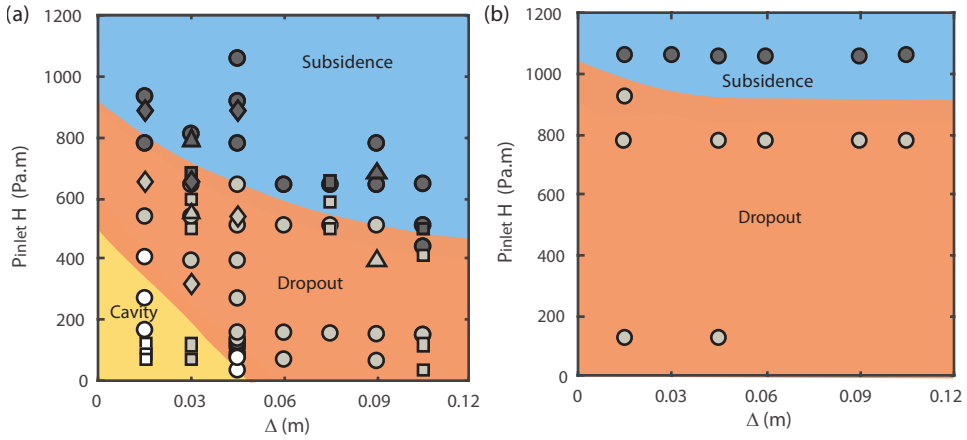

Figure 12: Phase diagrams related to the inlet pressure P_{inlet} multiply to H and the orifice size Δ, (a) for Coh=95, for different sample heights H=8.5 cm (square), 13.5 cm (circle) and 18.5 cm (triangle) when L=40 cm, and H=12.8 cm, L=23.7 cm (diamond). (b) Idem for Coh=191, L=23.7 cm and H=13.5 cm (circle).

3.2.3. Phase diagrams

Figures 11 and 12 present phase diagrams that locate the domains of existence of cavity formation, dropout sinkhole and subsidence sinkhole, according to inlet pressure P_{inlet}, orifice size Δ, sample height of H, sample length L and cohesion number Coh. Figure 11 shows two diagrams displaying P_{inlet} as a function of Δ for a fixed Coh, a fixed L, and two different sample heights of H=13.5 cm (a) and H=8.5 cm (b). For both cases, the erosion process successively jumps from cavity to dropout sinkhole and ultimately to subsidence sinkhole when P_{inlet} and Δ are increased. It can be seen that, for the range studied, the location of the frontier between two regimes depends on the height H of the granular sample. In an attempt to rationalize this dependency, we plotted (not shown here) the dimensionless pressure, dividing P_{inlet} by the hydrostatic pressure $\rho_f g H$, as a function of different dimensionless orifice sizes (using r, H or L). But in each case the regime transitions kept being influenced by H. In Figure 12a, we nevertheless found empirically that multiplying P_{inlet} by H leads to an approximate grouping of the different erosion regime frontiers, regardless

of the sample geometry (for various H and L) and for a given cohesion state. Although this result could have practical implications, we do not yet have any physical explanation for it. Finally, Figure 12b indicates that for a doubled Coh, a higher P_{inlet} and Δ are necessary to pass from dropout to subsidence sinkholes, and there is no longer any cavity formation within the same range of parameters.

3.2.4. Spatio-temporal diagrams

In this numerical study, we developed a post-processing tool to carry out a spatio-temporal analysis on the basis of our simulations. Figure 13 presents a typical image of the interparticle force network in its initial state. Using ImageJ, an open-source software application, we can select the main eroded zone corresponding to the orifice width (on the left image) to plot averaged spatio-temporal diagrams (on the right). Thus, the vertical axis of a diagram displays the mean pixel density calculated in the selected zone and the horizontal axis is time. Using this representation, clearly shows that the two erosion regimes mainly differ by their front propagation directions. The spatio-temporal diagram related to the dropout sinkhole shows an almost constant surface level with time, while the backward erosion advances from the bottom. Conversely, the subsidence sinkhole displays an almost linear decrease of the surface level with time. This difference in the induced ground motion (observed from the surface) is indeed that commonly agreed by the natural hazards community to distinguish dropout from subsidence sinkholes (Sowers, 1996).

3.3. Predictive analysis for dropout sinkholes

The objective of our research is to improve the prediction of where, why and when a sinkhole will occur. From the risk assessment viewpoint, the dropout sinkhole is the most critical one because cavity widening cannot be viewed directly from the surface. A relevant aspect of the micromechanical modeling we propose is precisely to give access to the internal evolution of the process. Therefore, we present here a qualitative first-order predictive analysis based on

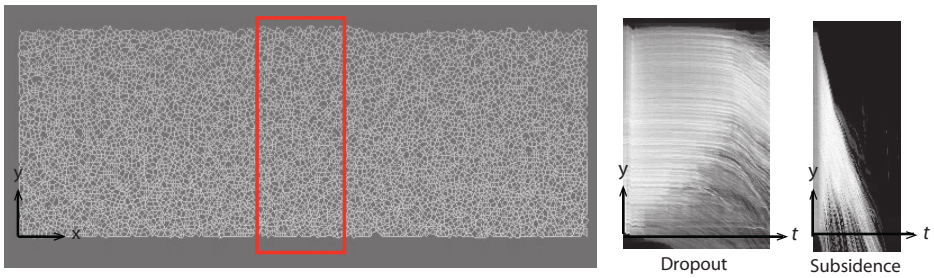

Figure 13: Typical spatio-temporal diagrams averaged within the central orifice zone (red frame), and showing typical evolutions for both dropout and subsidence sinkholes.

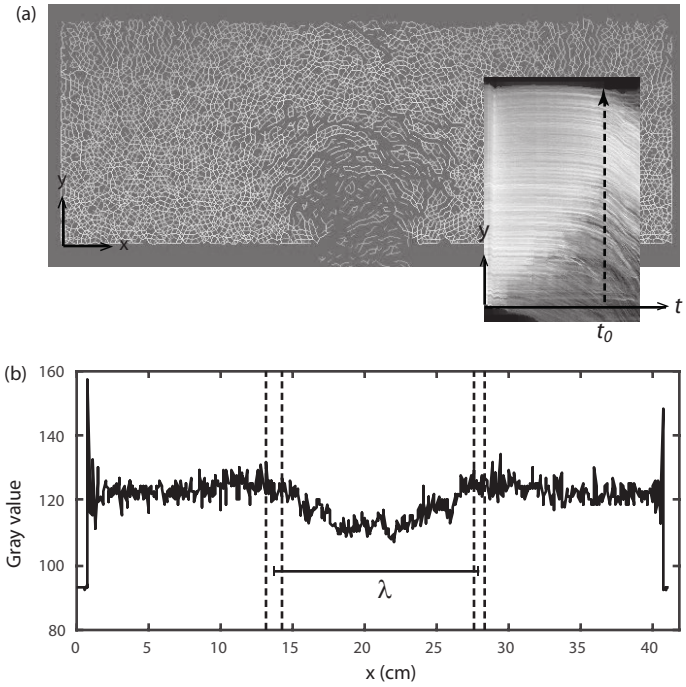

Figure 14: Dropout sinkhole case: (a) snapshot of interparticle bonds at the characteristic time t_0 indicated on the averaged spatio-temporal diagram. (b) *Plot Profile* (using ImageJ software) at t_0 and collapse width λ estimation (see text).

the numerical simulations of the backward erosion scenario.

As mentioned in the previous section dedicated to the field scenarios, Sowers proposed the geotechnical approach of considering a potential collapse diameter of 2/3 the height of the overlying soil layer (Sowers, 1996). This approach concerns the quasi-static growth of a void in a cohesive but non-submerged soil. Using our simulations, we propose to estimate the extension of bond breakage in a flood situation, when backward erosion occurs in a saturated soil under hydraulic loading. To this end, we perform a systematic procedure to characterize the maximum width of the eroded zone. On the spatio-temporal diagram presented previously, we detect a characteristic time t_0 at which the surface starts to cave-in, as indicated in Fig. 14a. At that moment $t = t_0$, we apply the *Plot Profile* function of ImageJ that displays a two-dimensional graph of the intensities of pixels along a line. The x-axis represents the horizontal distance and the y-axis the vertically averaged pixel intensity (Fig. 14b). Thus, we can estimate the so-called collapse width λ with acceptable measurement uncertainty.

By applying this image processing for typical simulations of the dropout sinkhole regime, we obtain the graph shown in Figure 15 (left). The collapse width λ is plotted as a function of the height of the granular sample H. The main finding is that λ is roughly equal to the cohesive soil thickness H (slope equal to 1), accounting for a moderate discrepancy and irrespectively of H, P_{inlet}, Δ and Coh. When considering second-order trends, we remark that the higher P_{inlet} and Δ are, the higher λ becomes. When Coh is doubled, λ is either slightly smaller or equal within the error bar.

With a first-order approximation, the simulations of the dynamic process in a flood situation therefore predict a linear relationship between the collapse size λ and the cover thickness H, according to Sower's prediction but with a higher slope of 1 instead of 2/3. In addition, we find that this result does not depend on the other parameters (P_{inlet}, Δ and Coh), therefore providing an interesting relationship for applications. In contrast, as expected, Figure 15 (right) indicates that the erosion kinetics depends on all the parameters studied. Indeed, by plotting t_0 the time at which the surface starts becoming destabilized

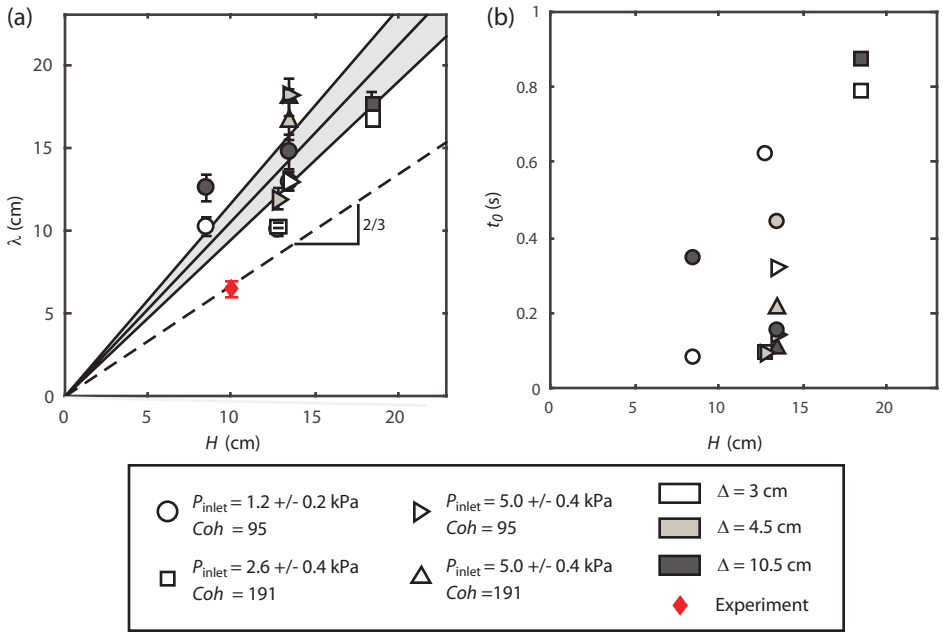

Figure 15: (a) Collapse width λ *vs* granular sample height H, for various inlet pressures P_{inlet}, orifice size Δ and particle cohesion Coh. Linear fit giving a slope equal to 1. The grey area indicates the 95% confidence bounds obtained on the slope. (b) The corresponding characteristic collapse time t_0.

(defined in Figure 14a) as a function of H, we observe a much broader spread of data than for λ. For a fixed H, whereas the maximum discrepancy for λ corresponds to a doubled value, the scatter of t_0 can reach up to a factor 6. A more systematic study would be necessary to capture the dependency of t_0 on the different parameters. Qualitatively, we observe that the higher P_{inlet} and Δ is, the faster the erosion. Inversely, the greater the H, the slower the erosion kinetics. In these simulations, particle cohesion seems to have little influence. Note that the estimation of the characteristic collapse time t_0 here gives only qualitative but not quantitative information on time scales. The next step would be to calibrate using real soil parameters to obtain a more realistic prediction of sinkhole dynamics, which would greatly improve risk management. Linking the numerical modeling illustrated here to geotechnical assessments will be a significant step toward characterizing sinkhole hazards.

4. Experimental modeling

In addition, we performed an exploratory experimental study to enrich the previous numerical results. An original methodology has recently been developed to produce artificial cohesive granular media similar to our numerical granular assemblies (Brunier-Coulin, 2016).

4.1. Materials and setup

For the present study, we use Hostun sand HN31 (mean diameter of 240 μm), which is a reference sand used in many experimental geotechnical studies. Solid bridges are created by "sticking" sand grains together with liquid paraffin. The amount of paraffin is chosen low enough to prevent the complete filling of voids between particles, in the sense that the liquid far from saturates the granular sample. We then paid particularly attention to the homogeneous mixing of the sand with hot liquid paraffin. When the mixture is cooled and the paraffin has solidified, we obtain an artificial cohesive granular material that can be considered as a weakly cemented sand.

The experimental setup is pictured in Figure 16. The cohesive sand is prepared in a specific sample cell open at the top and open only by a circular orifice at the bottom. For this study, we tested an orifice diameter between 1.5 cm and 2.5 cm. By filling this cell, we produced soil samples whose height varied between 10 cm and 12 cm, with a fixed length of 20 cm and a fixed width of 5.5 cm. This sample cell was then introduced into a larger (external) cell connected to a gear pump. This closed-loop system induced a controlled flow rate to continuously erode the granular sample with a downward water flow. During the erosion experiment, the sand was assumed to be evacuated through the output conduit connected to the upper reservoir. In all the experiments performed, we could see through the transparent plastic tube that eroded sand flowed out of the orifice without clogging the pipe. A primary saturation phase is crucial before erosion is triggered. Contrary to the flow direction for erosion ("input" to "output"), we allowed the water to rise very slowly from the bottom with the air being removed upwards. In this way, we were able to immerse all the pores in the granular matter.

4.2. Results

As can be seen in Figure 17, this rather simple setup nevertheless allowed us to simulate two regimes very similar to those observed in our numerical study and consistent with the field scenarios. However, regarding sand cohesion, we were unable to explore a wide range of paraffin concentrations, i.e. around 0.3% per weight for both examples. For higher values, the maximum pump flow rate was not high enough to erode the soil. For lower concentrations of paraffin, the cohesive sample was too easily weakened during its preparation and introduction in the setup, leading to fractures and even collapse when the eroding flow was imposed. Moreover, both processes were obtained with the same flow rate. Inhomogeneity in the sample was also identified. This could explain why we observed large aggregates and falling blocks. Therefore, as currently framed, the experimental conditions allowed us neither to precisely control the parameters nor to select one of the two regimes. Improvement of

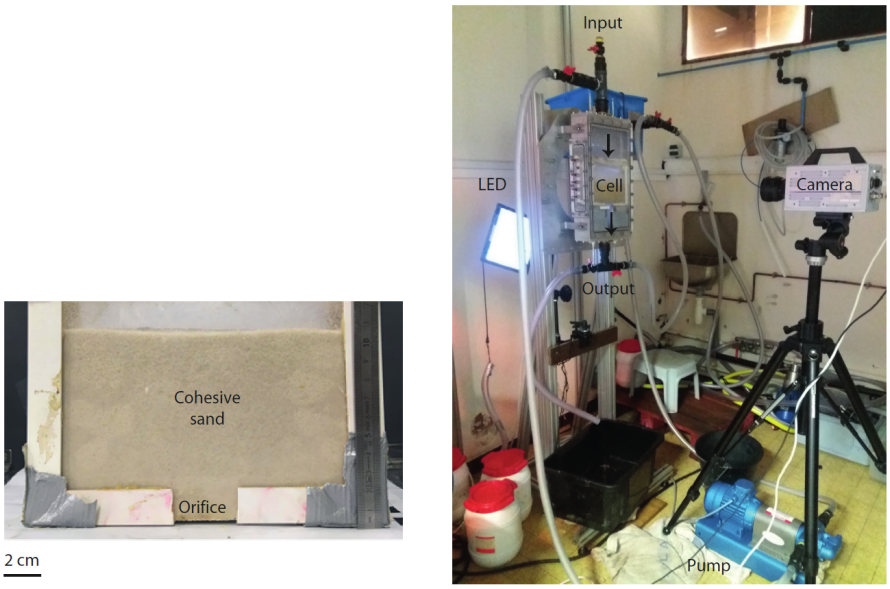

Figure 16: Experimental setup. Left: Sample cell. Right: hydraulic closed-loop (see text).

the protocol is in progress.

In spite of this, we were able to obtain an interesting result from the dropout sinkhole process. As indicated in Fig. 17 we estimated a characteristic damage size λ. As can be seen in Fig. 15 (red losange), this measurement is in good agreement with the prediction of Sowers (lower than predicted by our simulations, as discussed in 3.3), giving relevancy to this exploratory experimental study. In future work, to ensure better comparability with our numerical simulations, certain tests could be performed by varying the sand diameter to the cell width ratio in order to study the 3D effects. The next step will also focus on the calibration of parameters such as artificial interparticle cohesion using purely mechanical tests (traction test, direct shear), in order to make more quantitative comparisons between the experiments and simulations.

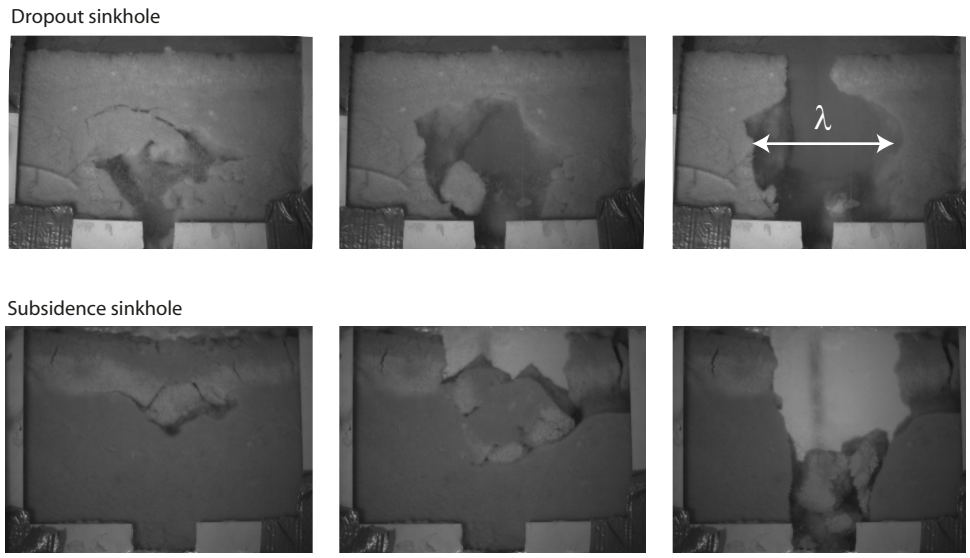

Figure 17: Typical experimental pictures of the two different erosion regimes. For the dropout and subsidence sinkhole, the sample height is equal to 10 cm and 12 cm, and the orifice diameter around 1.5 cm and 2.5 cm, respectively. The estimation of the maximum damage λ in the dropout sinkhole case is indicated.

5. Conclusion and perspectives

Sinkhole occurrences represent a major geohazard that remains poorly assessed, especially in exceptional flood situations. The meteorological event occurring in the Orléans area in spring 2016, is a relevant example of a huge increase in the number of cavity collapses. This paper presented a physical model of hydro-mechanical instabilities under hydraulic forcing on a cohesive soil layer underlain by a karstic cavity. The numerical study involving a coupled LBM-DEM method provided insight into the micromechanism of particle bond breakage during internal erosion processes. By varying hydraulic pressure, underground conduit size and the particle cohesion of the granular media, we identified two different erosion kinetics (excluding cavity formation), namely upward cavity development and downward granular discharge, leading to the formation of dropout and subsidence sinkholes (in cohesive soil), respectively. On the basis of a parametric study, we plotted a phase diagram to delimit the respective domain of each regime. Then, we performed systematic measurements, directly from our simulations, of the eroded zone when a dropout sinkhole occurred. We found a linear relationship between the characteristic collapse width and the height of the cohesive soil overlaying the underground conduit. This result demonstrated the ability of our calculations to reproduce an erosion process, consistent with classical geotechnics estimations of hypothetical sinkhole size. Finally, the first results of an experimental model demonstrated its capacity to produce similar sinkholes, as predicted by the field scenario and numerical simulations.

Following these results, one of the immediate future goals will be to integrate calibration in our numerical model. Further comparison between both numerical-experimental approaches will include transcribing the cohesion achieved in the laboratory tests (typically traction and shear tests) to the particle bond strength implemented in the cohesion model of our code. Linking this multiscale numerical model to geotechnical *in situ* conditions will be a significant step in characterizing sinkhole hazards and risks.

Acknowledgements

We thank André Benjamin (internship student) for his contribution to the experimental study. This research was funded by PERCIVAL (PErception des Risques effondrements liés aux Cavités associés aux Inondations en VAL de Loire), French Regional Research Program (2018-2020) attributed by the Centre-Val de Loire region.

References

Baryakh, A. A., Fedoseev, A. K., 2011. Sinkhole formation mechanism. Journal of Mining Science, 47(4), 404-412.

Beck, B., 2012. Soil piping and sinkhole failures. In Encyclopedia of Caves (Second Edition) (pp. 718-723).

Benahmed, N., Canou, J., Dupla, J. C., 2004. Initial structure and static liquefaction properties of sand. Comptes Rendus Mecanique, 332(11), 887-894.

Bonelli, S., 2013. Erosion in geomechanics applied to dams and levees. John Wiley Sons.

Bouzidi, M. H., Firdaouss, M., Lallemand, P., 2001. Momentum transfer of a Boltzmann-lattice fluid with boundaries. Physics of Fluids, 13(11), 3452-3459.

Brinkmann, R., Parise, M., Dye, D., 2008. Sinkhole distribution in a rapidly developing urban environment: Hillsborough County, Tampa Bay area, Florida. Engineering Geology, 99(3-4), 169-184.

Brunier-Coulin, F., 2016. Etude des mécanismes élémentaires de l'érosion d'un sol cohésif (Doctoral dissertation, Aix-Marseille).

Cuellar, P., Philippe, P., Bonelli, S., Benahmed, N., Brunier-Coulin, F., Ngoma, J., Radjai, F., 2015. Micromechanical analysis of the surface erosion of a cohesive soil by means of a coupled LBM-DEM model. In Proceedings of the International Conference on Particles, Barcelona, Spain (pp. 28-30).

Cundall, P. A., Strack, O. D. L. (1979). The development of constitutive laws for soil using the distinct element method. Numerical methods in geomechanics, 1, 289-317.

Delenne, J. Y., El Youssoufi, M. S., Cherblanc, F., Bénet, J. C., 2004. Mechanical behaviour and failure of cohesive granular materials. International Journal for Numerical and Analytical Methods in Geomechanics, 28(15), 1577-1594.

De Waele, J., Gutiérrez, F., Parise, M., Plan, L., 2011. Geomorphology and natural hazards in karst areas: a review. Geomorphology, 134(1-2), 1-8.

Ford, D., Williams, P. D., 2013. Karst hydrogeology and geomorphology. John Wiley Sons.

Gutiérrez, F., Parise, M., De Waele, J., Jourde, H., 2014. A review on natural and human-induced geohazards and impacts in karst. Earth-Science Reviews, 138, 61-88.

Hyatt, J. A., Jacobs, P. M., 1996. Distribution and morphology of sinkholes triggered by flooding following Tropical Storm Alberto at Albany, Georgia, USA. Geomorphology, 17(4), 305-316.

Iverson, R. M., 2000. Landslide triggering by rain infiltration. Water resources research. 36(7), 1897-1910.

Kuniansky, E. L., Weary, D. J., Kaufmann, J. E., 2016. The current status of mapping karst areas and availability of public sinkhole-risk resources in karst terrains of the United States. Hydrogeology Journal. May2016, Vol. 24 Issue 3, p613-624. 12p.

Lallemand, P., Luo, L. S., 2000. Theory of the lattice Boltzmann method : Dispersion, dissipation, isotropy, Galilean invariance, and stability. Physical Review E. 61(6), 6546.

Liu, P., LaMarche, C. Q., Kellogg, K. M., Hrenya, C. M., 2018. A square force cohesion model and its extraction from bulk measurements. AIChE Journal.

Lominé, F., Scholtès, L., Sibille, L., Poullain, P., 2013. Modeling of fluid-solid interaction in granular media with coupled lattice Boltzmann/discrete element

methods: Application to piping erosion. International Journal for Numerical and Analytical Methods in Geomechanics. 37, 577– 596.

Lorain, J. M., 1973. La géologie du calcaire de Beauce. Le Calcaire de Beauce. Bulletin de liaison des laboratoires des Ponts et Chaussées.

Luu, L.-H., Philippe, P., Noury, G., Perrin, J., Brivois, O., 2017. Erosion of cohesive soil layers above underground conduits. In EPJ Web of Conferences (Vol. 140, p. 09038). EDP Sciences.

Moreau, J., 2002. Les gouffres du nord d'Orléans. Groupe spéléologique orléanais. Bulletin, 7, 1-28.

Ngoma, J., Philippe, P., Bonelli, S., Radjaï, F., Delenne, J. Y., 2018. Two-dimensional numerical simulation of chimney fluidization in a granular medium using a combination of discrete element and lattice Boltzmann methods. Physical Review E, 97(5), 052902.

Noury, G., Perrin, J., Luu, L. H., Philippe, P., Gourdier, S., 2018. Role of floods on sinkholes occurence in covered karst terrains: Case study of Orléans area (France) during the 2016 meteorological events and perspectives for other karst environments. In 15th Multidisciplinary Conference on Sinkholes and the Engineering and Environmental Impacts of Karst.

Perez, A. L., Nam, B., Chopra, M., Sallam, A., 2017. Understanding Florida's Sinkhole Hazards: Hydrogeological Laboratory Study. In Geotechnical Frontiers 2017 (pp. 508-518).

Perrin, J., Cartannaz, C., Noury, G., Vanoudheusden, E., 2015. A multicriteria approach to karst subsidence hazard mapping supported by weights-of-evidence analysis. Engineering Geology, 197, 296-305.

Perrin, J, Pasquier S, Gutierrez A, Salquebre D, Vanoudheusden E, Joigneaux E, Binet S., 2017. -Investigating physical processes leading to sinkhole occurrence in Val d'Orléans (France). In EuroKarst 2016, Neuchâtel (pp. 79–86). Springer, Cham.

Radjaï, F., Dubois, F., 2011. Discrete-element modeling of granular materials (pp. 425-p). Wiley-Iste.

Rawal, K., Hu, L. B., Wang, Z. M., 2017. Numerical investigation of the geomechanics of sinkhole formation and subsidence. In Geotechnical Frontiers 2017 (pp. 480-487).

Sellmeijer, H., de la Cruz, J. L., van Beek, V. M., Knoeff, H., 2011. Fine-tuning of the backward erosion piping model through small-scale, medium-scale and IJkdijk experiments. European Journal of Environmental and Civil Engineering, 15(8), 1139-1154.

Silvani, C., Désoyer, T., Bonelli, S., 2009. Discrete modelling of time-dependent rockfill behaviour. International journal for numerical and analytical methods in geomechanics, 33(5), 665-685.

Shalev, E., Lyakhovsky, V., 2012. Viscoelastic damage modeling of sinkhole formation. Journal of Structural Geology, 42, 163-170.

Sowers, G. F., 1996. Building on sinkholes: design and construction of foundations in karst terrain. American Society of Civil Engineers.

Talon, L., Bauer, D., Gland, N., Youssef, S., Auradou, H., Ginzburg, I., 2012. Assessment of the two relaxation time Lattice-Boltzmann scheme to simulate Stokes flow in porous media. Water Resources Research, 48(4).

Tao, X., Ye, M., Wang, X., Wang, D., Pacheco Castro, R., Zhao, J., 2015. Experimental and Numerical Investigation of Sinkhole Development and Collapse in Central Florida.

Tran, D. K., Prime, N., Froiio, F., Callari, C., Vincens, E., 2017. Numerical modelling of backward front propagation in piping erosion by DEM-LBM coupling. European Journal of Environmental and Civil Engineering, 21(7-8), 960-987.

Waltham, T., 2008. Sinkhole hazard case histories in karst terrains. Quarterly Journal of Engineering Geology and Hydrogeology, 41(3), 291-300.

Wilson, G. V., Rigby, J. R., Dabney, S. M., 2015. Soil pipe collapses in a loess pasture of Goodwin Creek watershed, Mississippi: role of soil properties and past land use. Earth Surface Processes and Landforms, 40(11), 1448-1463.

Yu, D., Mei, R., Luo, L. S., Shyy, W., 2003. Viscous flow computations with the method of lattice Boltzmann equation. Progress in Aerospace Sciences, 39(5), 329-367.